

Thermoelectric properties of β -As, Sb and Bi monolayers

Dong-Chen Zhang, Ai-Xia Zhang and San-Dong Guo

School of Physics, China University of Mining and Technology, Xuzhou 221116, Jiangsu, China

Monolayer semiconductors of group-VA elements (As, Sb, Bi) with graphenelike buckled structure offer a potential to achieve nanoscale electronic, optoelectronic and thermoelectric devices. Motivated by recently-fabricated Sb monolayer (antimonene), we systematically investigate the thermoelectric properties of β -As, Sb and Bi monolayers by combining the first-principles calculations and semiclassical Boltzmann transport theory. The generalized gradient approximation (GGA) plus spin-orbit coupling (SOC) is adopted for the electron part, and GGA is employed for the phonon part. It is found that SOC has important influences on their electronic structures, especially for Bi monolayer, which can induce observable SOC effects on electronic transport coefficients. More specifically, SOC not only has detrimental influences on electronic transport coefficients, but also produces enhanced effects. The calculated lattice thermal conductivity decreases gradually from As to Bi monolayer, and the corresponding room-temperature sheet thermal conductance is 161.10 WK^{-1} , 46.62 WK^{-1} and 16.02 WK^{-1} , which can be converted into common lattice thermal conductivity by dividing by the thickness of 2D material. The sheet thermal conductance of Bi monolayer is lower than one of other 2D materials, such as semiconducting transition-metal dichalcogenide monolayers and orthorhombic group IV-VI monolayers. A series of scattering time is employed to estimate the thermoelectric figure of merit ZT . It is found that the n-type doping has more excellent thermoelectric properties than p-type doping for As and Bi monolayer, while the comparative ZT between n- and p-type doping is observed in Bi monolayer. These results can stimulate further experimental works to open the new field for thermoelectric devices based on monolayer of group-VA elements.

PACS numbers: 72.15.Jf, 71.20.-b, 71.70.Ej, 79.10.-n

Keywords: Graphenelike buckled structure; β -As, Sb and Bi monolayers; Power factor; Thermal conductivity

I. INTRODUCTION

Due to high mobility, heat conductance, and mechanical strength, graphene with a planar honeycomb structure is one of the most famous materials, but it lacks an intrinsic band gap, hindering its applications in electronics and optoelectronics¹. The successful exfoliation of graphene intrigues a large number of search for further two-dimensional (2D) materials like silicene², germanene³, phosphorene⁴ and transition-metal dichalcogenides⁵, etc. Recently, monolayer semiconductors of group-VA elements (As, Sb, Bi) are predicted to be of good stability with intrinsic gap by the first-principle calculations, and the graphenelike buckled structure (β -phase) has the best stability⁶. The Sb monolayer (antimonene) of them has been successfully exfoliated through micromechanical technology⁷, or has been synthesized on various substrates via van der Waals epitaxy growth⁸. Experimentally, it has been proved that Sb monolayer is highly stable in ambient conditions⁷, and the high stability has been observed after aging in air for 30 days⁸. Raman spectroscopy and transmission electron microscopy show that the Sb monolayer has graphenelike buckled structure^{7,8}. It is urgent and interesting to study thermoelectric properties of Sb monolayer in detail, to determine whether it is a potential thermoelectric material.

Thermoelectric materials, which can achieve direct hot-electricity conversion without moving parts, are of great interest in energy-related issues^{9,10}. The efficiency of thermoelectric conversion can be measured by di-

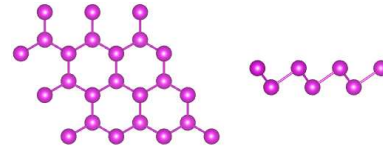


FIG. 1. The crystal structures of β -As, Sb and Bi monolayers: the top view (Left) and the side view (Right).

mensionless figure of merit, $ZT = S^2\sigma T/(\kappa_e + \kappa_L)$, in which S , σ , T , κ_e and κ_L are the Seebeck coefficient, electrical conductivity, working temperature, the electronic and lattice thermal conductivities, respectively. It is believed that nanostructured materials, especially for 2D materials, have potential application in highly efficient thermoelectric devices^{11–15}. The thermoelectric properties of semiconducting transition-metal dichalcogenide monolayers and orthorhombic group IV-VI monolayers have been widely investigated^{16–21}. Recently, our calculated results show that SOC can produce important effects on electronic transport coefficients of various 2D materials^{19,21–23}, so it is necessary for thermoelectric properties of 2D materials to include SOC. For group-VA monolayers, most of the research are focused on their lattice thermal conductivities, and their electronic transports are little investigated. The lattice thermal conductivities of As and Sb monolayers with both graphenelike buckled and black phosphorenelike puckered honeycomb structures (α -phase) have been performed in theory^{24–27}. A highly anisotropic thermal conductivity along the zigzag and armchair directions is predicted for

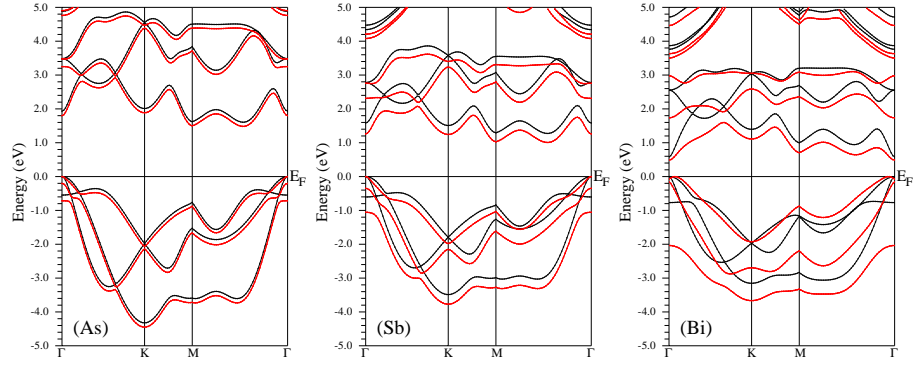


FIG. 2. The energy band structures of β -As, Sb and Bi monolayers within GGA (Black lines) and GGA+SOC (Red lines).

α -As and Sb monolayers^{25,26}. It has also been proved that chemical functionalization can make κ_L of Sb monolayer decrease greatly²⁷. The thermoelectric performance of α -As monolayer has been studied with Green's function based transport techniques, including both electron and phonon parts²⁸. It is noteworthy that a remarkable discrepancy between ref.²⁴ and ref.²⁵ for κ_L of β -Sb monolayer can be found. It may be because the different thickness of Sb monolayer is used, and the related discussion for calculations of transport coefficients of 2D materials can be found in the next section (computational detail).

Here, we investigate systematically the thermoelectric properties of β -As, Sb and Bi monolayers from ab initio calculations in combination with Boltzmann transport equation formalism, including both electron and phonon parts. The SOC is considered for electron part, which is very important for electronic structures and transport coefficients of β -As, Sb and Bi monolayers, especially for Bi monolayer. The lattice thermal conductivities using the same thickness and sheet thermal conductances of β -As, Sb and Bi monolayers are calculated, and they gradually decreases from As to Bi monolayer. It is found that the sheet thermal conductance of Bi monolayer is lower than one of familiar 2D materials. Finally, possible ZT is estimated by a series of empirical scattering time, which suggests that β -As, Sb and Bi monolayers may be potential 2D thermoelectric materials.

The rest of the paper is organized as follows. In the next section, we shall describe computational details about the first-principle and transport coefficients calculations. In the third section, we shall present the electronic structures and thermoelectric properties of β -As, Sb and Bi monolayers. Finally, we shall give our discussions and conclusion in the fourth section.

II. COMPUTATIONAL DETAIL

We use a full-potential linearized augmented-plane-waves method within the density functional theory (DFT)²⁹ to carry out electronic structures of β -As,

TABLE I. The lattice constants a (Å) and buckling parameter h (Å)⁶; the calculated gap values using GGA G (eV) and GGA+SOC G_{so} (eV); $G-G_{so}$ (eV); spin-orbit splitting $\Gamma_{\Delta_{so}}$ and $K_{\Delta_{so}}$ (eV) at the high symmetry point Γ and K of valence bands.

Name	a	h	G	G_{so}	$G-G_{so}$	$\Gamma_{\Delta_{so}}$	$K_{\Delta_{so}}$
As	3.61	1.40	1.61	1.48	0.13	0.21	0.07
Sb	4.12	1.65	1.27	1.01	0.26	0.35	0.17
Bi	4.34	1.73	0.58	0.49	0.09	0.08	0.77

Sb and Bi monolayers, as implemented in the package WIEN2k³⁰. The free atomic position parameters are optimized using GGA of Perdew, Burke and Ernzerhof (GGA-PBE)³¹ with a force standard of 2 mRy/a.u.. The SOC is included self-consistently³²⁻³⁵, which gives rise to important influences on electronic transport coefficients. The convergence results are determined by using 5000 k-points in the first Brillouin zone (BZ) for the self-consistent calculation, making harmonic expansion up to $l_{\max} = 10$ in each of the atomic spheres, and setting $R_{\text{mt}} * k_{\max} = 8$ for the plane-wave cut-off. The self-consistent calculations are considered to be converged when the integration of the absolute charge-density difference between the input and output electron density is less than $0.0001|e|$ per formula unit, where e is the electron charge.

Based on the results of electronic structure, transport coefficients for electron part are calculated through solving Boltzmann transport equations within the constant scattering time approximation (CSTA), as implemented in BoltzTrap³⁶, which shows reliable results in many classic thermoelectric materials³⁷⁻³⁹. To obtain accurate transport coefficients, we set the parameter LPFAC for 20, and use at least 2408 k-points in the irreducible BZ for the energy band calculation. The lattice thermal conductivities are performed by using Phono3py+VASP codes⁴⁰⁻⁴³. The second order harmonic and third order anharmonic interatomic force constants are calculated by using a $5 \times 5 \times 1$ supercell and a $4 \times 4 \times 1$ supercell, respectively. To compute lattice thermal conductivities,

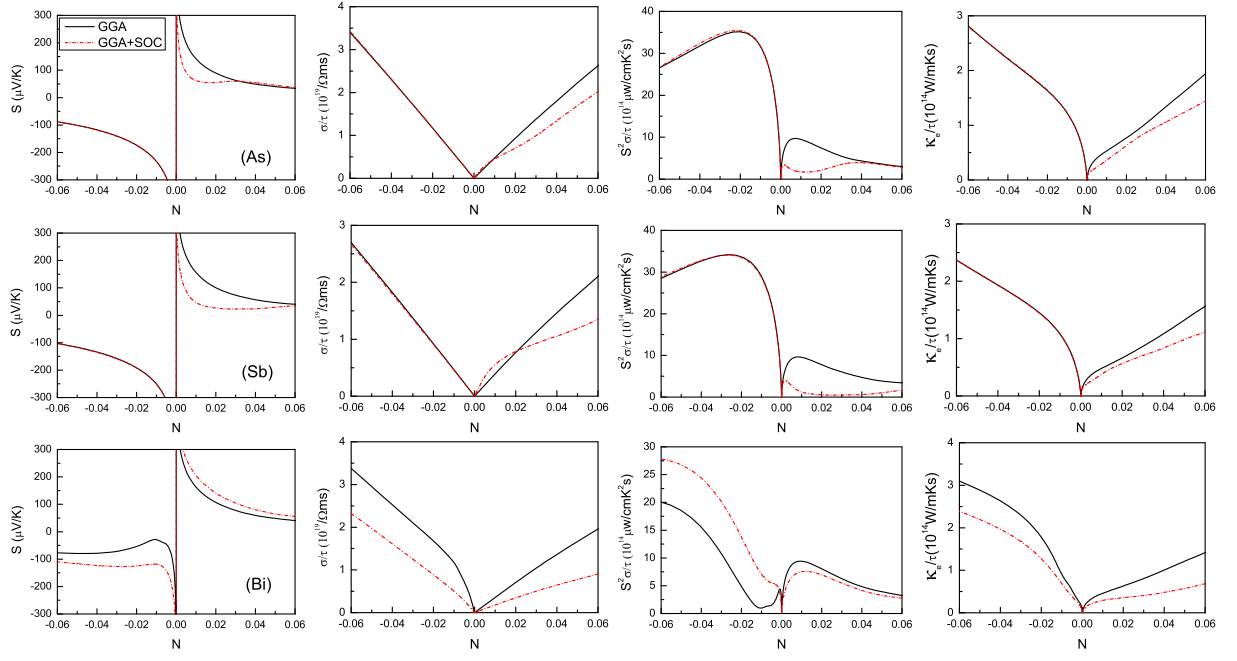


FIG. 3. (Color online) At room temperature (300 K), transport coefficients of β -As, Sb and Bi monolayers as a function of doping level (N) within GGA and GGA+SOC: Seebeck coefficient S , electrical conductivity with respect to scattering time σ/τ , power factor with respect to scattering time $S^2\sigma/\tau$ and electronic thermal conductivity with respect to scattering time κ_e/τ .

the reciprocal spaces of the primitive cells are sampled using the $50 \times 50 \times 2$ meshes.

For 2D material, the calculated electrical conductivity, electronic and lattice thermal conductivities depend on the length of unit cell used in the calculations along z direction⁴⁴, which should be normalized by multiplying L_z/d , where L_z is the length of unit cell along z direction and d is the thickness of 2D material, but the d is not well defined. However, The dimensionless figure of merit ZT is independent of the length of unit cell used in the calculations along z direction. In this work, the length of unit cell used in our calculations along z direction is used as the thickness of β -As, Sb and Bi monolayers, and the corresponding d is 18 Å. The thermal sheet conductance can be used as a fair comparison between various 2D monolayers, which can be attained by $\kappa \times d$.

III. MAIN CALCULATED RESULTS AND ANALYSIS

The β -phase of As, Sb and Bi monolayers is a graphenelike buckled honeycomb structure with space group of $P\bar{3}m1$ (No. 164), and the schematic crystal structure is shown in Figure 1. The β -phase is different from α -phase with puckered honeycomb structure. The unit cell of β -phase contains two atoms with each atom connected to three atoms of another plane, while α -phase contains four atoms with each atom connected to two atoms of the same plane and one atom of another plane.

In this work, the optimized lattice constants of β -phase are used⁶, which are summarized in Table I. It is found that the buckling parameter h from Table I, defined as the vertical distance separating the two atomic planes, gradually increases from As to Bi monolayer. The unit cell of β -As, Sb and Bi monolayers is constructed with the vacuum region of larger than 16 Å to avoid spurious interaction. As is well known, the SOC has very important effects on electronic structures and electronic transport coefficients of materials containing heavy element^{19,21–23}, such as Bi. Firstly, the electronic structures of β -As, Sb and Bi monolayers are investigated using GGA and GGA+SOC, and the energy band structures are plotted in Figure 2 using GGA and GGA+SOC. The As and Sb monolayers are indirect band gap semiconductors with the valence band maximum (VBM) at the Γ point and conduction band minimum (CBM) at the M point using both GGA and GGA+SOC. The Bi monolayer is a direct band gap semiconductor with VBM and CBM at the Γ point using GGA, while it is an indirect band gap semiconductors with VBM between the Γ and M points and CBM at the Γ point using GGA+SOC. The GGA and GGA+SOC gaps, and the differences between them are listed in Table I. Both GGA and GGA+SOC gaps decrease from As to Bi monolayer, and the difference of Bi monolayer is less than ones of As and Sb monolayers, which is due to the change of CBM from M to Γ point. The three monolayers have some conduction band extrema (CBE) around the Fermi level, which is favorable for n-type Seebeck coefficient. According to SOC-

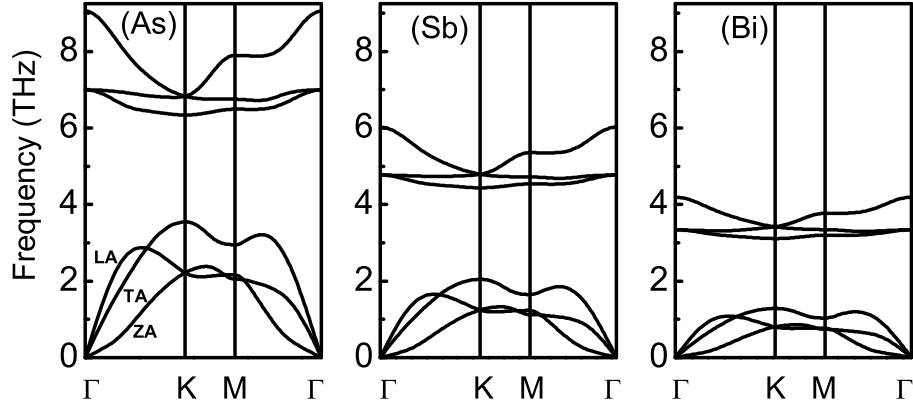


FIG. 4. Phonon band structure of β -As, Sb and Bi monolayers using GGA-PBE.

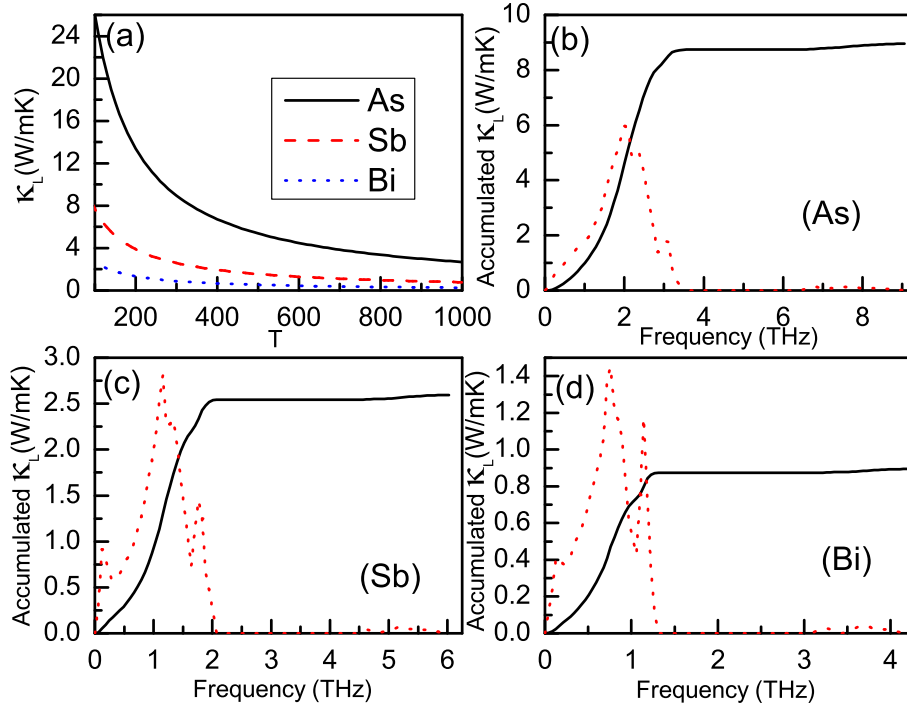


FIG. 5. (a) The lattice thermal conductivities of β -As, Sb and Bi monolayers as a function of temperature using GGA-PBE. (b), (c) and (d) The accumulated lattice thermal conductivities of β -As, Sb and Bi, and the derivatives.

induced changes of outlines of energy bands, the strength of SOC increases from As to Bi monolayer, which is consistent with their respective atomic mass. The representative spin-orbit splitting values at the high symmetry points Γ and K of valence bands are summarized in Table I. It is found that the spin-orbit splitting value at K point can represent the strength of SOC.

The SOC can produce very important effects on electronic transport coefficients in many 2D materials, such as semiconducting transition-metal dichalcogenide and orthorhombic group IV-VI monolayers^{19,21–23}. Firstly, the semi-classic transport coefficients are calculated within CSTA Boltzmann theory using GGA and GGA+SOC, and the doping effects are simulated by sim-

ply shifting the Fermi level into conduction or valence bands within rigid band approach, which is valid with the doping level being low^{45–47}. The Seebeck coefficient S , electrical conductivity with respect to scattering time σ/τ , power factor with respect to scattering time $S^2\sigma/\tau$ and electronic thermal conductivity with respect to scattering time κ_e/τ as a function of doping level (N) at room temperature are plotted in Figure 3 using GGA and GGA+SOC.

For As and Sb monolayers, it is found that SOC has a detrimental effect on Seebeck coefficient in p-type doping, while has a negligible influence in n-type doping. The detrimental effect can be explained by SOC-induced splitting at Γ point, which reduces the degeneracy of en-

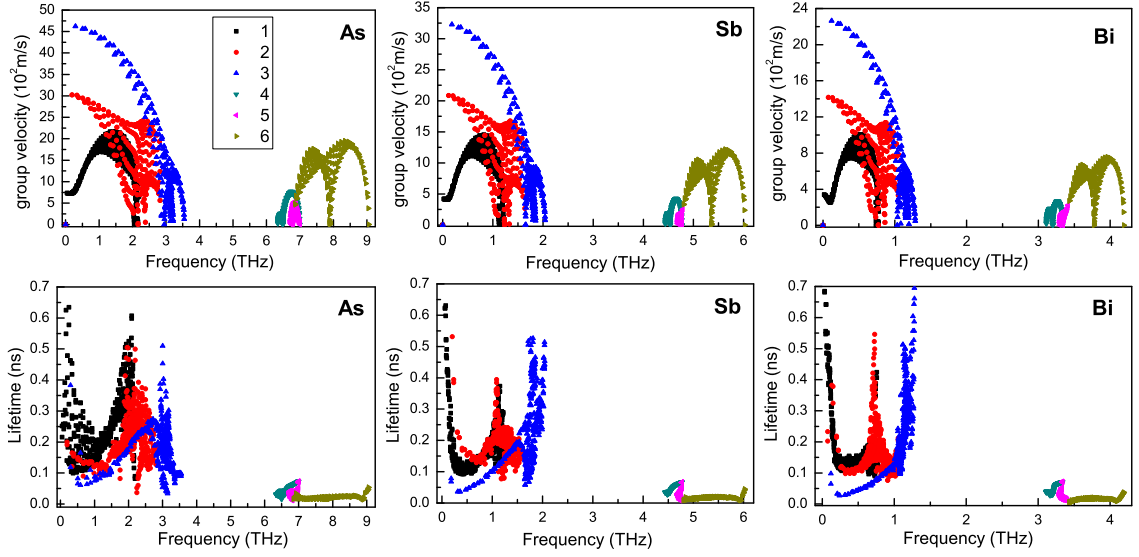


FIG. 6. (Color online) Calculated phonon group velocities and phonon lifetimes of β -As, Sb and Bi monolayers using GGA-PBE in the irreducible Brillouin zone. 1 represents ZA branch, 2 for TA branch, 3 for LA branch and 4, 5, 6 for optical branches.

ergy bands. However, the enhanced effect on Seebeck coefficient (absolute value) can be observed in both n- and p-type doping for Bi monolayer, which can be understood by bands convergence⁹. At presence of SOC, the CBE along Γ -M and CBM approach each other, which leads to improved n-type Seebeck coefficient. When SOC is considered, the VBM changes from Γ point to one point along Γ -M, and another valence band extrema (VBE) appears at one point along Γ -K. The VBE along Γ -K and VBM are very close, and the energy difference only is 0.0005 eV, which gives rise to enhanced p-type Seebeck coefficient.

TABLE II. The maximal acoustic vibration frequency $MAVF$ (THz), width of optical branches WO (THz), phonon band gap PBG (THz), thermal sheet conductance TSC (WK^{-1}), acoustic branch contribution to lattice thermal conductivity ACL (%) and corresponding frequency of peak value of derivatives FPD (THz).

Name	$MAVF$	WO	PBG	TSC	ACL	FPD
As	3.55	2.71	2.79	161.10	97.6	2.01
Sb	2.05	1.58	2.39	46.62	98.1	1.06
Bi	1.29	1.08	1.82	16.02	98.1	0.76

In n-type doping, a neglectful influence on σ/τ of As and Sb monolayers can be observed at the presence of SOC, while a slightly improved effect in low p-type doping and a detrimental influence in high p-type doping can be achieved. For Bi monolayer, a decreased effect on σ/τ caused by SOC in both n- and p-type doping can be observed. The effect on $S^2\sigma/\tau$ of As and Sb monolayers induced by SOC has the same trend with one on S. A enhanced effect in n-type doping and a decreased influence in p-type doping on $S^2\sigma/\tau$ of Bi monolayer produced by

SOC can be fulfilled. It is found that the effect on κ_e/τ caused by SOC has almost similar trend with one on σ/τ , which can be explained by the Wiedemann-Franz law: $\kappa_e = L\sigma T$, in which L is the Lorenz number.

Based on the linearized phonon Boltzmann equation within single-mode relaxation time approximation, the lattice thermal conductivities of β -As, Sb and Bi monolayers can be attained, which are assumed to be independent of doping level. Their phonon band structures are shown in Figure 4, which agree well with previous results⁶. Their unit cell contains two atoms, resulting in 3 acoustic and 3 optical phonon branches. From As to Bi monolayer, the whole branches move toward low energy, and the phonon dispersion becomes more localized. The maximal acoustic vibration frequency (MAVF) is 3.55 THz, 2.05 THz and 1.29 THz from As to Bi monolayer, and a low MAVF is benefit to low thermal conductivity. The width of optical branches of β -As, Sb and Bi monolayers is 2.71 THz, 1.58 THz and 1.08 THz, respectively, and the narrow width suggests little contribution to thermal conductivity. The third optical branch has larger dispersion than the first two ones, which means the third one has larger group velocity, leading to obvious contribution to lattice thermal conductivity. The phonon band gap decreases from As (2.79 THz) to Sb (2.39 THz) to Bi (1.82 THz) monolayer. It is found that the longitudinal acoustic (LA) and transverse acoustic (TA) branches are linear near the Γ point, while the z-direction acoustic (ZA) branch deviates from linearity near the Γ point, which shares the general feature of 2D materials^{48,49}. The related data are summarized Table II.

The lattice thermal conductivities of β -As, Sb and Bi monolayers as a function of temperature are shown in Figure 5, and the same thickness d (18 Å) is used. The room-temperature lattice thermal conductivity of β -As,

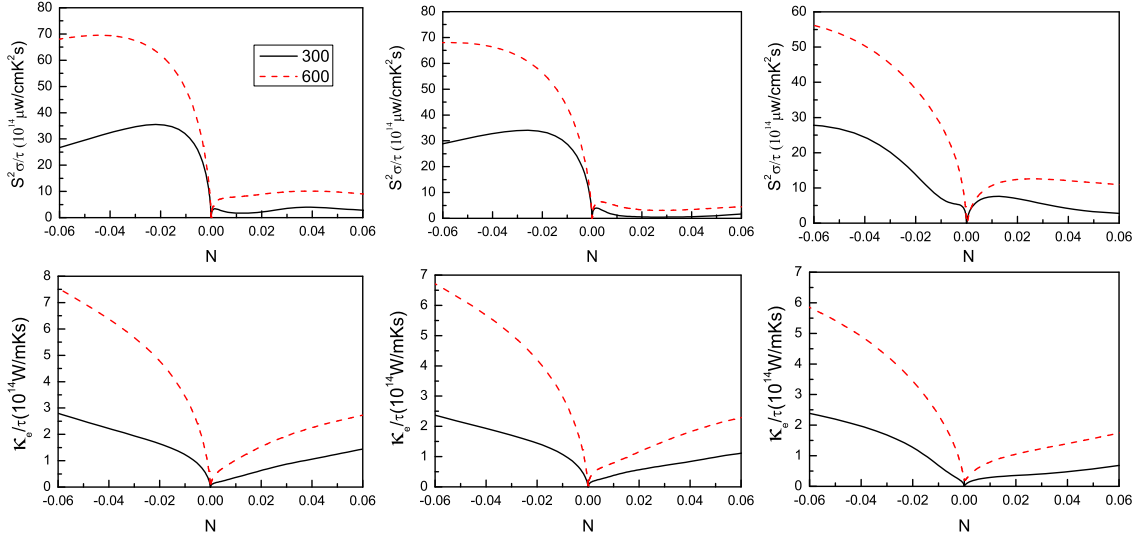


FIG. 7. (Color online) At 300 and 600 K, the power factor with respect to scattering time $S^2\sigma/\tau$ and electronic thermal conductivity with respect to scattering time κ_e/τ versus doping level (N) using GGA+SOC.

TABLE III. At 300 K, the phonon mode and total lattice thermal conductivities of β -As, Sb and Bi monolayers, including acoustic (ZA, TA and LA) and optical (O1, O2 and O3) branches. Unit: ($\text{Wm}^{-1}\text{K}^{-1}$).

Name	ZA	TA	LA	O1	O2	O3	κ_L
As	2.927	3.109	2.702	0.032	0.013	0.169	8.952
Sb	0.630	1.086	0.826	0.009	0.001	0.043	2.594
Bi	0.247	0.360	0.266	0.004	0.001	0.016	0.894

Sb and Bi monolayers is $8.95 \text{ Wm}^{-1}\text{K}^{-1}$, $2.59 \text{ Wm}^{-1}\text{K}^{-1}$ and $0.89 \text{ Wm}^{-1}\text{K}^{-1}$, respectively. To compare the lattice thermal conductivities of various 2D materials, we convert all thermal conductivity values into thermal sheet conductance⁴⁴, and the corresponding thermal sheet conductance is 161.10 WK^{-1} , 46.62 WK^{-1} and 16.02 WK^{-1} , respectively. The thermal sheet conductance of Bi monolayer is lower than one of other 2D materials (semiconducting transition-metal dichalcogenide and orthorhombic group IV-VI monolayers), and is very close to ones of SnS (18.68 WK^{-1}) and SnSe (17.55 WK^{-1})⁴⁴. To examine the relative contributions of acoustic modes to the total lattice thermal conductivity, the cumulative lattice thermal conductivity and the derivatives are also plotted in Figure 5 at room temperature. The acoustic branch of β -As, Sb and Bi monolayers provides a contribution of 97.6%, 98.1% and 98.1%, respectively. This meets the usual picture that high-frequency optical phonons have very little contribution to thermal conductivity. The derivatives show that the change of lattice thermal conductivity versus frequency has a peak value, and the corresponding frequency of peak value is 2.01 THz, 1.16 THz and 0.76 THz from As to Bi monolayer. These frequencies and cross values of ZA and LA branches almost

overlap. Some key data are shown in Table II. Furthermore, we examine the relative contributions of six phonon modes to the total lattice thermal conductivity, and the mode lattice thermal conductivities are shown Table III. It is found that TA branch provides the largest contribution in acoustic branches, and the third optical branch gives the greatest contribution in optical ones.

According to Figure 6, the group velocity of ZA branch is smaller than ones of LA and TA branches, which is due to nonlinear dispersion of ZA branch near the Γ point. It is clearly seen that group velocities become small from As to Bi monolayer, which leads to a decrescent thermal conductivity. The largest group velocity for ZA, TA and LA branches near Γ point is 0.73 kms^{-1} , 3.03 kms^{-1} and 4.62 kms^{-1} for As monolayer, 0.42 kms^{-1} , 2.08 kms^{-1} and 3.24 kms^{-1} for Sb monolayer, 0.34 kms^{-1} , 1.42 kms^{-1} and 2.26 kms^{-1} for Bi monolayer. The phonon lifetimes of β -As, Sb and Bi monolayers at room temperature are plotted in Figure 6. As can be seen, most of the phonon lifetimes are decrease from As to Bi monolayer, which can explain decreasing lattice thermal conductivity. It is found that optical phonon lifetimes are very shorter than acoustic ones, which suggests that optical branches has little contribution to lattice thermal conductivity.

Based on calculated electron and phonon transport coefficients, the figure of merit ZT can be attained to estimate the efficiency of thermoelectric conversion. Firstly, the power factor with respect to scattering time $S^2\sigma/\tau$ and electronic thermal conductivity with respect to scattering time κ_e/τ versus doping level (N) using GGA+SOC at 300 and 600 K are plotted in Figure 7. However, another unknown quantity is scattering time τ , but it is difficulty to calculate scattering time from the first-principle calculations due to the complexity of various carrier scattering mechanisms. Here, $1 \times 10^{-15} \text{ s}$, $1 \times 10^{-14} \text{ s}$ and $1 \times 10^{-13} \text{ s}$ are used to attain the power fac-

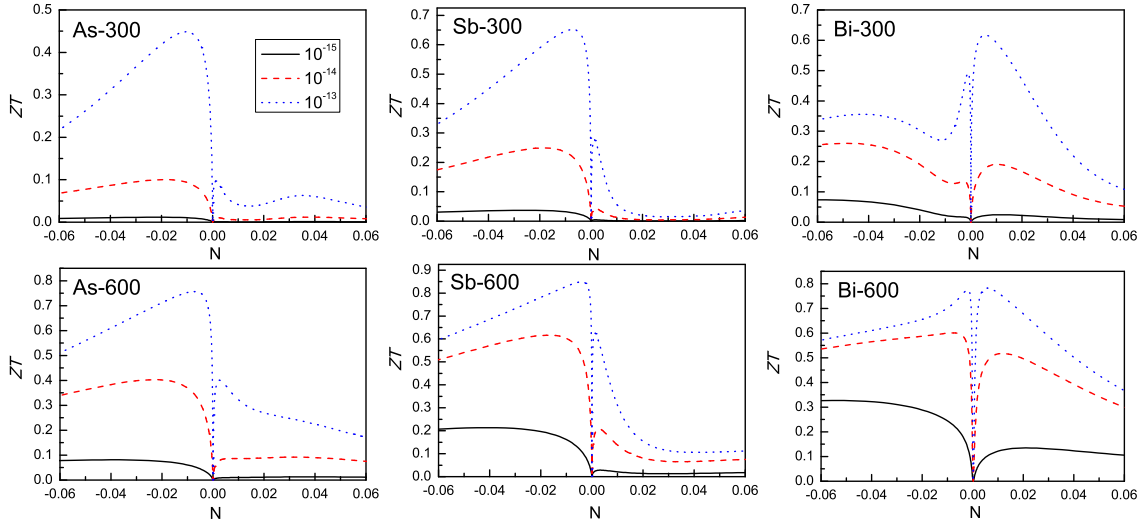


FIG. 8. (Color online) At 300 and 600 K, calculated ZT of β -As, Sb and Bi monolayers as a function of doping level with the scattering time τ being 1×10^{-15} s, 1×10^{-14} s and 1×10^{-13} s.

tor and electronic thermal conductivity. According to attained power factor, electronic thermal conductivity and lattice thermal conductivity from Figure 5, the possible ZT of β -As, Sb and Bi monolayers as a function of doping level at 300 and 600 K are plotted in Figure 8. It is found that ZT increases with increased scattering time τ , which can be explained by the relation: $ZT = ZT_e \times \kappa_e / (\kappa_e + \kappa_L)$, in which $ZT_e = S^2 \sigma T / \kappa_e$ as an upper limit of ZT . The κ_e can be attained by $\kappa_e / \tau_r \times \tau$, in which τ_r , τ are true and empirical scattering time, respectively. As the scattering time τ increases, the κ_e increases. That leads to that the $\kappa_e / (\kappa_e + \kappa_L)$ is more close to one, and then ZT is closer to ZT_e . Calculated results show that the n-type doping for As and Sb monolayers has more excellent ZT than p-type doping, and that Bi monolayer shows almost equivalent ZT between n- and p-type doping. It is found that a peak ZT in n-type doping is up to 0.40, 0.62 and 0.60 from As to Bi monolayer with classic scattering time $\tau = 10^{-14}$ s, and the corresponding doping level gradually decreases. These imply that β -As, Sb and Bi monolayers may be potential 2D thermoelectric materials by optimizing doping.

IV. DISCUSSIONS AND CONCLUSION

Seebeck coefficient can be tuned by removing or enhancing band degeneracy, and further can affect power factor. For β -As, Sb and Bi monolayers, the SOC removes not only band degeneracy (orbital degeneracy), but also enhance one (valley degeneracy). The SOC can lead to reduced effects on the p-type Seebeck coefficient of As and Sb monolayers by lifting the degenerate of Γ point, but can enhance Seebeck coefficient of Bi monolayer due to bands converge caused by spin-orbit splitting. Similar SOC effects on Seebeck coefficient are also

found in semiconducting transition-metal dichalcogenide monolayers MX_2 ($M = \text{Zr, Hf, Mo, W}$ and Pt ; $X = \text{S, Se}$ and Te)²³. The observably enhanced effects on Seebeck coefficient can be observed in monolayers WX_2 ($X = \text{S, Se}$ and Te), and detrimental effects in MX_2 ($M = \text{Zr, Hf, Mo}$ and Pt ; $X = \text{S, Se}$ and Te). For bulk materials, the detrimental effects on Seebeck coefficient caused by SOC also can be found in Mg_2X ($X = \text{Si, Ge, Sn}$)^{50,51} and half-Heusler ANiB ($A = \text{Ti, Hf, Sc, Y}$; $B = \text{Sn, Sb, Bi}$)⁵². Therefore, including SOC is very important for electronic transport coefficients of β -As, Sb and Bi monolayers.

The electronic structures of 2D materials is quite sensitive to strain, and β -As, Sb and Bi monolayers have some CBE around the Fermi level. So, it is possible to tune their thermoelectric properties by band engineering. Strain (pressure) has been proved to be a very effective strategy to improve thermoelectric properties of 2D (bulk) materials^{19,22,51,53}. For bulk Mg_2Sn , pressure can induce accidental degeneracies (orbital degeneracy) of CBM, which can significantly improve power factor⁵¹. Strain-enhanced power factor can also be found in monolayer MoS_2 ²², PtSe_2 ¹⁹ and ZrS_2 ⁵³ due to bands converge (valley degeneracy) induced by strain. It has also been proved that tensile strain can reduce lattice thermal conductivity in many 2D materials, such as PtSe_2 ¹⁹, PtTe_2 ⁵⁴ and ZrS_2 ⁵³. It has been predicted that strain can induce bands converge in As monolayer⁵⁵. Therefore, strain effects on thermoelectric properties of β -As, Sb and Bi monolayers are well worth studying. It has been predicted that the perpendicular electric field can induce an indirect-to-direct gap transition of As monolayer at 4.2 V/nm by the first-principle calculations⁵⁵, which suggests that the electric field can also tune the electronic structures. Therefore, it is possible to tune electronic transport properties of β -As, Sb and Bi monolayers by electric field.

TABLE IV. A ($\text{Wm}^{-1}\text{K}^{-1}$): Lattice thermal conductivity using the same thickness of the interlayer distance of graphite (3.35 Å). B (WK^{-1}): Thermal sheet conductance.

Name	GeS	GeSe	SnS	SnSe	ZrS ₂	ZrSe ₂	HfS ₂	HfSe ₂	As	Sb	Bi
A	15.80	9.43	5.58	5.24	23.25	18.55	29.06	20.71	48.09	13.74	4.78
B	52.93	31.58	18.68	17.55	77.89	62.14	97.35	69.38	161.10	46.62	16.02

The potential thermoelectric materials should possess low lattice thermal conductivity. To compare the lattice thermal conductivities of different monolayer 2D materials, the same thickness d should be adopted, or the sheet thermal conductance should be used⁴⁴. Here, the same thickness of the interlayer distance of graphite (3.35 Å) is used⁴⁴. The lattice thermal conductivities and sheet thermal conductances of β -As, Sb and Bi monolayers, some semiconducting transition-metal dichalcogenide monolayers and orthorhombic group IV-VI monolayers are summarized in Table IV. The lattice thermal conductivity of Bi monolayer is lower than that of orthorhombic group IV-VI monolayers and semiconducting transition-metal dichalcogenide monolayers, which suggests that it may be a potential 2D thermoelectric material compared to other familiar 2D materials. The lattice thermal conductivity of Sb monolayer has been widely calculated, for example $15.1 \text{ Wm}^{-1}\text{K}^{-1}$ ²⁴, $13.8 \text{ Wm}^{-1}\text{K}^{-1}$ ²⁵ and $2.3 \text{ Wm}^{-1}\text{K}^{-1}$ ²⁷. This apparent contradiction may be because the different thickness is used to calculate lattice thermal conductivity.

In conclusion, we have carried out a detailed theoretical studies of the thermoelectric properties of β -As, Sb and Bi monolayers based on ab initio calculations com-

bined with Boltzman transport theory. It is proved that SOC has important effects on electronic properties of β -As, Sb and Bi monolayers, which has been ignored in other theoretical calculations^{6,55}. The sheet thermal conductance is used to compare lattice thermal conductivities of different 2D materials, and the sheet thermal conductance of Bi monolayer is lower than one of other well-studied 2D materials, being very favorable to realize high thermoelectric efficiency. Finally, a series of hypothetical scattering time is adopted to estimate possible efficiency of thermoelectric conversion. Our work suggests that these β -As, Sb and Bi monolayers with graphene-like buckled structure may offer a new 2D playground to achieve high-performance thermoelectric devices.

ACKNOWLEDGMENTS

This work is supported by the National Natural Science Foundation of China (Grant No. 11404391). We are grateful to the Advanced Analysis and Computation Center of CUMT for the award of CPU hours to accomplish this work.

-
- ¹ A. H. Castro Neto, F. Guinea, N. M. R. Peres, K. S. Novoselov, and A. K. Geim, *Rev. Mod. Phys.* **81**, 109 (2009).
 - ² B. Aufray, A. Kara, S. Vizzini, H. Oughaddou, C. Landri, B. Ealet and G. Le Lay, *Appl. Phys. Lett.* **96**, 183102 (2010).
 - ³ L. Li, Y. Yu, G. J. Ye, Q. Ge, X. Ou, H. Wu, D. Feng, X. H. Chen and Y. Zhang, *Nature Nanotech.* **9**, 372 (2014).
 - ⁴ H. Liu, A. T. Neal, Z. Zhu, Z. Luo, X. Xu, D. Tomnek and P. D. Ye, *ACS Nano* **8**, 4033 (2014).
 - ⁵ G. Cunningham, M. Lotya, C. S. Cucinotta, S. Sanvito, S. D. Bergin, R. Menzel, M. S. P. Shaffer and J. N. Coleman, *ACS Nano* **6**, 3468 (2012).
 - ⁶ S. L. Zhang et al., *Angew. Chem.* **128**, 1698 (2016).
 - ⁷ P. Ares et al., *Adv. Mater.* **28**, 6332 (2016).
 - ⁸ J. P. Ji et al., *Nat. Commun.* **7**, 13352 (2016).
 - ⁹ Y. Pei, X. Shi, A. LaLonde, H. Wang, L. Chen and G. J. Snyder, *Nature* **473**, 66 (2011).
 - ¹⁰ A. D. LaLonde, Y. Pei, H. Wang and G. J. Snyder, *Mater. Today* **14**, 526 (2011).
 - ¹¹ L. Hicks and M. Dresselhaus, *Phys. Rev. B* **47**, 12727 (1993).
 - ¹² L. Hicks, T. Harman and M. Dresselhaus, *Appl. Phys. Lett.* **63**, 3230 (1993).
 - ¹³ Y. Xu, Z. Li, W. Duan, *Small* **10**, 2182 (2014).
 - ¹⁴ J. P. Heremans, M. Dresselhaus, L. E. Bell and D. T. Morelli, **8**, 471 (2013).
 - ¹⁵ M. Dresselhaus et al., *Adv. Mater.* **19**, 1043 (2007).
 - ¹⁶ S. Kumar and U. Schwingenschlög, *Chem. Mater.* **27**, 1278 (2015).
 - ¹⁷ J. Wu et al. *Nano Lett.* **14**, 2730 (2014).
 - ¹⁸ Z. Jin et al. *Sci. Rep.* **5**, 18342 (2015).
 - ¹⁹ S. D. Guo, *J. Mater. Chem. C* **4**, 9366 (2016).
 - ²⁰ F. Q. Wang, S. Zhang, J. Yu and Q. Wang, *Nanoscale* **7**, 15962 (2015).
 - ²¹ S. D. Guo and Y. H. Wang, *J. Appl. Phys.* **121**, 034302 (2017).
 - ²² S. D. Guo, *Comp. Mater. Sci.* **123**, 8 (2016).
 - ²³ S. D. Guo and J. L. Wang, *Semicond. Sci. Tech.* **31**, 095011 (2016).
 - ²⁴ S. D. Wang, W. H. Wang and G. J. Zhao, *Phys. Chem. Chem. Phys.* **18**, 31217 (2016).
 - ²⁵ G. H. Zheng, Y. L. Jia, S. Gao and S. H. Ke, *Phys. Rev. B* **94**, 155448 (2016).
 - ²⁶ M. Zeraati, S. M. V. Allaei, I. A. Sarsari, M. Pourfath, and D. Donadio, *Phys. Rev. B* **93**, 085424 (2016).
 - ²⁷ T. Zhang, Y. Y. Qi, X. R. Chen and L. C. Cai, *Phys. Chem. Chem. Phys.* **18**, 30061 (2016).

- ²⁸ L. M. Sandonas, D. Teich, R. Gutierrez, T. Lorenz, A. Pechia, G. Seifert and G. Cuniberti, *J. Phys. Chem. C* **120**, 18841 (2016).
- ²⁹ P. Hohenberg and W. Kohn, *Phys. Rev.* **136**, B864 (1964); W. Kohn and L. J. Sham, *Phys. Rev.* **140**, A1133 (1965).
- ³⁰ P. Blaha, K. Schwarz, G. K. H. Madsen, D. Kvasnicka and J. Luitz, WIEN2k, an Augmented Plane Wave + Local Orbitals Program for Calculating Crystal Properties (Karlheinz Schwarz Technische Universität Wien, Austria) 2001, ISBN 3-9501031-1-2
- ³¹ J. P. Perdew, K. Burke and M. Ernzerhof, *Phys. Rev. Lett.* **77**, 3865 (1996).
- ³² A. H. MacDonald, W. E. Pickett and D. D. Koelling, *J. Phys. C* **13**, 2675 (1980).
- ³³ D. J. Singh and L. Nordstrom, *Plane Waves, Pseudopotentials and the LAPW Method*, 2nd Edition (Springer, New York, 2006).
- ³⁴ J. Kunes, P. Novak, R. Schmid, P. Blaha and K. Schwarz, *Phys. Rev. B* **64**, 153102 (2001).
- ³⁵ D. D. Koelling, B. N. Harmon, *J. Phys. C Solid State Phys.* **10**, 3107 (1977).
- ³⁶ G. K. H. Madsen and D. J. Singh, *Comput. Phys. Commun.* **175**, 67 (2006).
- ³⁷ B. L. Huang and M. Kaviani, *Phys. Rev. B* **77**, 125209 (2008).
- ³⁸ L. Q. Xu, Y. P. Zheng and J. C. Zheng, *Phys. Rev. B* **82**, 195102 (2010).
- ³⁹ J. J. Pulikkotil, D. J. Singh, S. Auluck, M. Saravanan, D. K. Misra, A. Dhar and R. C. Budhani, *Phys. Rev. B* **86**, 155204 (2012).
- ⁴⁰ G. Kresse, *J. Non-Cryst. Solids* **193**, 222 (1995).
- ⁴¹ G. Kresse and J. Furthmüller, *Comput. Mater. Sci.* **6**, 15 (1996).
- ⁴² G. Kresse and D. Joubert, *Phys. Rev. B* **59**, 1758 (1999).
- ⁴³ A. Togo, L. Chaput and I. Tanaka, *Phys. Rev. B* **91**, 094306 (2015).
- ⁴⁴ X. F. Wu, V. Varshney et al., *Chem. Phys. Lett.* **669**, 233 (2017).
- ⁴⁵ T. J. Scheidemantel, C. Ambrosch-Draxl, T. Thonhauser, J. V. Badding and J. O. Sofo, *Phys. Rev. B* **68**, 125210 (2003).
- ⁴⁶ G. K. H. Madsen, *J. Am. Chem. Soc.* **128**, 12140 (2006).
- ⁴⁷ X. Gao, K. Uehara, D. Klug, S. Patchkovskii, J. Tse and T. Tritt, *Phys. Rev. B* **72**, 125202 (2005).
- ⁴⁸ H. Zabel, *J. Phys.: Condens. Matter* **13**, 7679 (2001).
- ⁴⁹ A. H. Castro Neto, F. Guinea, N. M. R. Peres, K. S. Novoselov and A. K. Geim, *Rev. Mod. Phys.* **81**, 109 (2009).
- ⁵⁰ K. Kutorasinski, B. Wiendlocha, J. Tobola and S. Kaprzyk, *Phys. Rev. B* **89**, 115205 (2014).
- ⁵¹ S. D. Guo and J. L. Wang, *RSC Adv.* **6**, 31272 (2016).
- ⁵² S. D. Guo, *J. Alloy. Compd.* **663**, 128 (2016).
- ⁵³ H. Y. Lv, W. J. Lu, D. F. Shao, H. Y. Lub and Y. P. Sun, *J. Mater. Chem. C* **4**, 4538 (2016).
- ⁵⁴ S. D. Guo, arXiv:1611.04119 (2016).
- ⁵⁵ C. Kamal and Motohiko Ezawa, *Phys. Rev. B* **91**, 085423 (2015).